3D long-range triplet migration in a water-stable metal-organic framework for upconversion based ultralow-power in vivo imaging

Jihye Park, Ming Xu, Fuyou Li, and Hong-Cai Zhou

J. Am. Chem. Soc., **Just Accepted Manuscript** • DOI: 10.1021/jacs.8b01613 • Publication Date (Web): 10 Apr 2018

3D long-range triplet migration in a water-stable metal–organic framework for upconversion based ultralow-power *in vivo* imaging

Jihye Park[1,†,§], Ming Xu[2,†], Fuyou Li[2,*], and Hong-Cai Zhou[1,*]

[1]Department of Chemistry, Texas A&M University, College Station, TX 77843-3255, USA.

[2]Department of Chemistry & State Key Laboratory of Molecular Engineering of Polymers, Fudan University, Shanghai 200433, P. R. China.

ABSTRACT: Triplet-triplet annihilation upconversion (TTA-UC) has gained increasing attention because it allows for harvesting of low energy photons in the solar spectrum with high efficiency in relevant applications including solar cells and bioimaging. However, the utilization of conventional TTA-UC systems for low-power bio-applications is significantly hampered by their general incompatibility and low efficiency in aqueous media. Herein we report a metal–organic framework (MOF) as a biocompatible nanoplatform for TTA-UC to realize low power *in vivo* imaging. Our MOF consists of a porphyrinic sensitizer in an anthracene-based Zr-MOF as a TTA-UC platform. In particular, closely aligned chromophores in the MOF facilitate a long-range 3D triplet diffusion of 1.6 μm allowing efficient energy migration in water. The tunable ratio between sensitizer and annihilator by our synthetic method also allows an optimization of the system for maximized TTA-UC efficiency in water at a very low excitation power density. Consequently, the low-power imaging of lymph node in a live mouse was successfully demonstrated with an excellent signal-to-noise ratio (SNR > 30 at 5 mW cm^{-2}).

INTRODUCTION

As a unique imaging technique where low photon energy is employed, photon upconversion (UC) processes have gained growing attention.[1] In particular, the upconversion process is well suited for biological imaging because the utilization of low photon energy can prevent tissue damages and *in vivo* autofluorescence from anti-Stokes shift.[2] The most widely applied technology to date, rare-earth metal based upconversion nanophosphors (RE-UCNPs), have been widely employed to obtain high contrast images with high a signal-to-noise ratio (SNR).[3-4] However, RE-UCNPs often suffer from low absorption cross-section and poor upconversion luminescence quantum efficiency, which in turn undesirably requires a high power input (~ few W cm^{-2}).[5] Therefore, an upconversion system that can be operated at a low power density is highly desired, particularly for biological specimens. In this regard, triplet-triplet annihilation based upconversion (TTA-UC) has emerged as an ideal alternative that can accommodate a low excitation power density, tunable photophysical properties on the molecular level, and high upconversion quantum efficiency.[6]

TTA-UC system typically comprises a pair of chromophores (dyad): sensitizer and annihilator. Upon photoexcitation of a sensitizer, a singlet state sensitizer undergoes intersystem crossing (ISC), giving rise to its triplet state. Then triplet-triplet annihilation between two excited triplet annihilators generated by triplet-triplet energy transfer (TTET, from sensitizer to annihilator) eventually populates as one excited singlet annihilator. Subsequently, the upconverted emission is then observed in higher energy than the initial input. Since the TTET and TTA processes heavily rely on triplet diffusion, the energy migration facilitated by high mobility of triplet excitons plays an important role for the overall TTA-UC performance.[7-9] Typically, in non-viscous organic solvents where chromophores can freely diffuse to promote the energy migration, a reasonable TTA-UC efficiency can be achieved with the excitation power as low as the solar irradiance.[10-11] However, the incompatibility of organic solvents with biological samples prompted the search for TTA-UC systems in aqueous media. For instance, incorporation of TTA-UC dyads has been formulated in amphiphilic polymers or micelles to enable their upconversion luminescence in aqueous media.[12-14] However, the trade off in these approaches is often a slowdown of triplet diffusion rate due to the limited mobility of the dissolved chromophores in such matrices. Meanwhile, the annihilator and sensitizer in these systems usually adopt a random orientation and an uncontrolled distance between one another, resulting in insufficient intermolecular excitonic couplings. These intrinsic disadvantages inevitably impair the efficient energy transfer, thus greatly lowering the TTA-UC efficiency. As a consequence, an undesirably high excitation power was necessary for bioimaging (~ 0.1 W cm^{-2}), which lowers the practicality of TTA-UC technique with increased risk of organ damage.[12-14] Therefore, development of a water stable TTA-UC system with a controlled orientation of the chromophores for efficient energy migration is highly desired for the low-power bioimaging.

Recently, metal–organic frameworks (MOFs) have captured widespread research interests in biological applications because of their synthetic tunability and improved chemical stability in aqueous media.[15] Furthermore, MOFs have been explored as a promising energy transfer (ET) platform that can realize a cooperative molecular-level function due to their highly accessible and spatially discrete linkers in the framework.[16-19] Apart from the well-defined arrangement of chromophores, the luminescence quenching from aggregation can also be prevented when such emissive dyes are used as the strut of MOFs. Therefore, water stable MOFs can serve as an ideal TTA-UC platform to facilitate efficient energy migration under physiological conditions. Herein we report the first example of a biocompatible TTA-UC MOF that demonstrates a low-power *in vivo* imaging. With an *in situ* secondary functionality incorporation, a sensitizer, Pd(II)-meso-tetrakis(4-carboxyphenyl)porphyrin (Pd-TCPP) was incorporated into a water stable Zr-MOF, constructed from an annihilator linker, 4,4'-(9,10-anthracenediyl)dibenzoic acid (DCDPA). The efficient triplet diffusion was successfully demonstrated in water, exhibiting a diffusion constant comparable to that of molecular systems in organic solvents and a diffusion length on the micrometer scale. Because our synthetic strategy allows a fine-tuning of the ratios between the sensitizer and annihilator,[20] the system was optimized for the highest TTA-UC efficiency in water measured at solar irradiance. Consequently, the TTA-UC MOF capable of working at ultralow excitation power was successfully employed for real-time lymph node imaging with a remarkable signal-to-noise ratio *in vivo*.

RESULTS AND DISCUSSION

Design of the water-stable TTA-UC MOFs. When incorporating cooperative functionalities in a MOF, such as a TTA-UC dyad, a pillar-layered structure with M_2 paddlewheel (M = Zn, Cu) can be easily considered through the mixed-linker strategy (Supporting Information Scheme S2).[21] In pillar-layered structures, one chromophore forms 2D layers while another chromophore connects the 2D layers as pillars. However, M_2 paddlewheels-based MOFs are typically unstable in aqueous media due to lability of their coordination bonds. Thus, a successful MOF for TTA-UC must consider the chemical stability of the MOFs to utilize the structural features of MOFs without degradation.

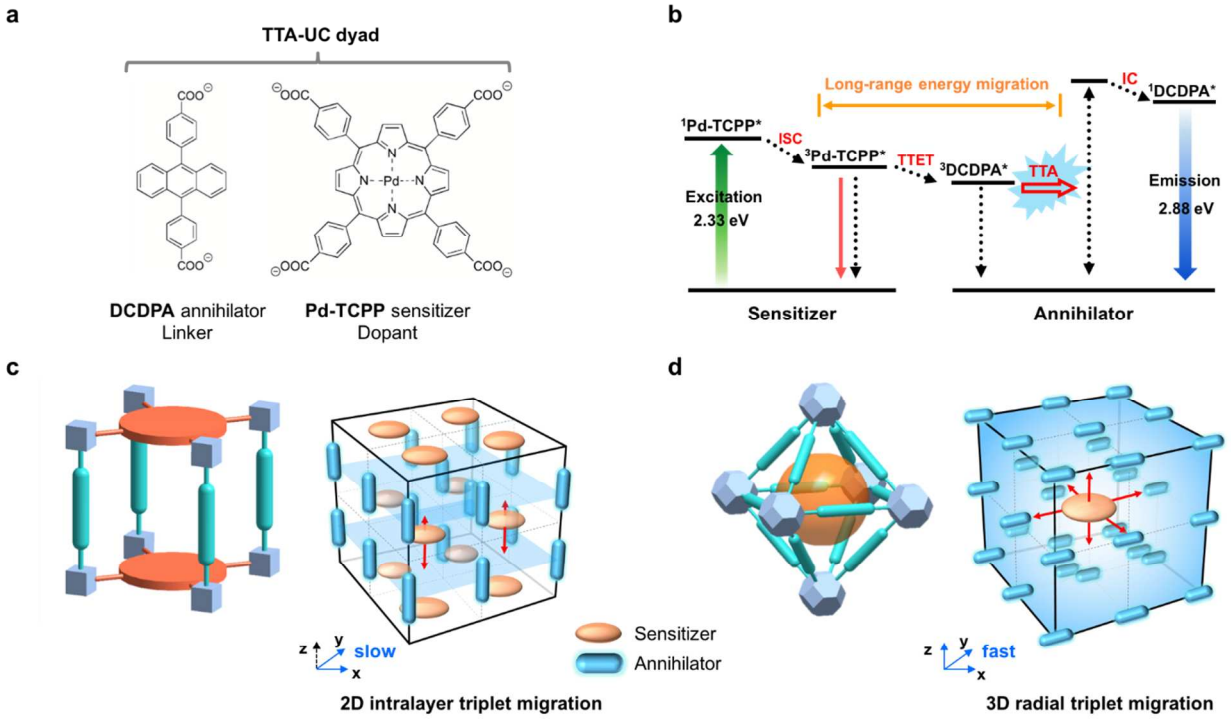

Figure 1 | Structural analysis and the triplet energy migration pathways in different types of TTA-UC MOFs. a, Chemical structures of annihilator and sensitizer to construct TTA-UC MOF. **b**, A schematic of the proposed TTA-UC process in TTA-UC system of Pd-TCPP/DCDPA. **c**, Proposed schematic of TTA-UC system based on a conventional pillar-layered MOF (left) and the spatial distribution of the TTA-UC chromophores allowing 2D intralayer triplet migration (right). The cyan represents the annihilator, the orange represents the sensitizer, respectively as linkers. The light blue cubes represent paddlewheel clusters. **d**, Proposed schematic of TTA-UC system based on a UiO-68 analogue (left) and the spatial distribution of TTA-UC chromophores allowing 3D triplet migration (right). The orange sphere in UiO-68 cage represents an accessible void space. The light blue cuboctahedra represent Zr_6 clusters. (**c**,**d**) The red arrows represent TTET from sensitizers to annihilators and the blue planes represent ET and TTA between adjacent annihilators.

Based on our design, the TTA-UC in the MOF platform is schematically represented in Figure 1b. The TTA-UC process involves multiple steps of energy transfers complying Dexter exchange mechanism, which is sensitive to orbital overlaps (Figure 1b and Supporting Information Scheme S1).[22] Therefore, proper distance and placement between chromophores are of crucial importance when designing a TTA-UC system (Supporting Information Section 1). In that regard, MOFs can be a promising candidate to realize a precise placement of chromophores. However, there are two drawbacks in possible MOF designs with pillar-layered structure. First, with the chosen TTA-UC dyad, the large porphyrinic sensitizer will result in a large distance between annihilator layers, which would hamper an effective triplet migration between 2D layers (Supporting Information Scheme S2). Moreover, the ratio between sensitizer and annihilator is intrinsically determined by the structure, disabling the ratio tuning between annihilator and sensitizer which could be an accessible method to screen high TTA-UC efficiency.[6,23] Therefore, achieving highly efficient TTA-UC in a water-stable MOF platform for bioimaging remains a great challenge.

To address these challenges, herein we propose a new nanoplatform to realize a 3D fast triplet migration in water where TTA-UC dyad is incorporated into a Zr-MOF nanoparticle through *in situ* insertion of functional defects.[20] In our design, an anthracene-based annihilator (DCDPA) is employed as a linker to construct the Zr-MOF (Figures 1a and 1d). Then, the secondary functionality (carboxylated tetratopic sensitizer, Pd-TCPP) is introduced through *in situ* coordination to defective coordination sites of Zr_6 clusters $[Zr_6O_4(OH)_4(COO)_{12}]$ in the MOF (Figure 2a). With this method, the concentration of the sensitizer can be finely tuned upon varying feed ratios in the MOF synthesis, which yields a Pd-TCPP doped UiO-68 analogue (Figure 2b). The high connectivity of UiO-68, defined as 2,12-connected **fcu-a** net allows many sub-networks or available coordination sites on the Zr_6 cluster in the MOF without destruction of the framework.[24-27] Therefore, our synthetic strategy is particularly suited for TTA-UC as it often requires a screening of the annihilator to sensitizer ratio to find a maximum upconversion efficiency of the system.

In particular, due to high connectivity of the Zr_6 cluster in our MOF, the annihilators are highly populated and aligned along all directions, providing a well-aligned 3D π orbital path in the framework for efficient diffusion of triplet excitons.[28] For instance, each annihilator in the framework is surrounded by eight neighboring annihilators (Figures 1d and 2a), which can increase the probability of effective TTA-UC process, compared to the possible pillar-layered structures that can only have four neighboring anthracenes (Figure 1c and Supporting Information Scheme S2). Meanwhile, when the sensitizer was incorporated into the framework, it is likely to be fully surrounded by the annihilators with radial proximity, thus further facilitating TTET process and providing 3D pathways of fast triplet migration (Figures 1d and 2b). Most importantly, since the framework is based on robust Zr(IV)-carboxylate bonds, the aggregation of chromophores can be prevented by retention of the framework in aqueous media.

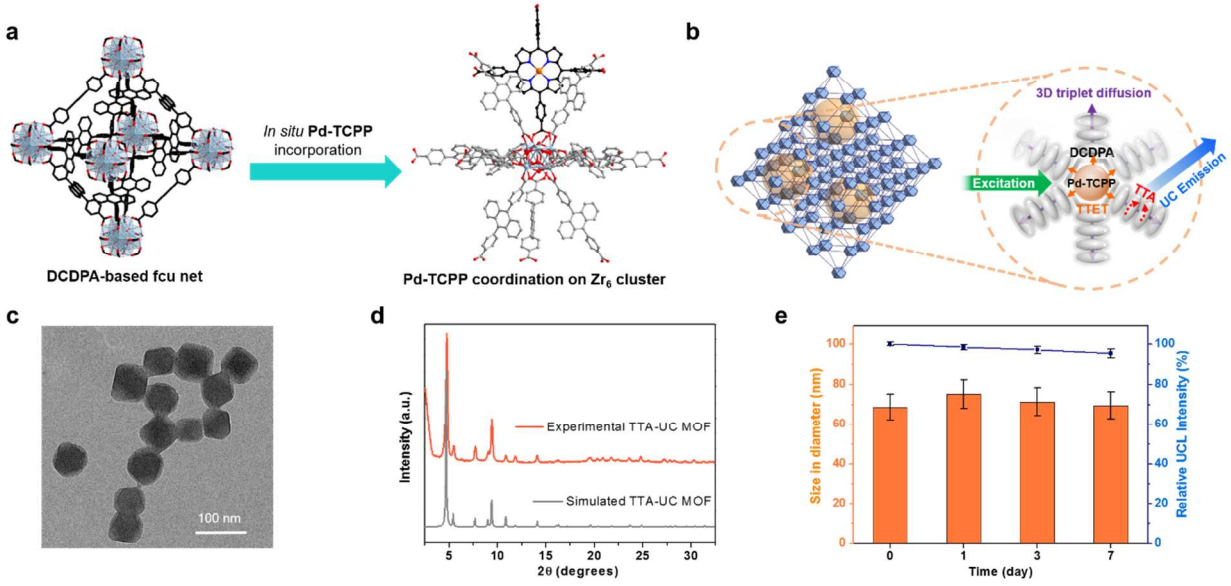

Figure 2 | Structure of and characterizations of TTA-UC MOF 5. a, *In situ* incorporation of Pd-TCPP into DCDPA MOF matrix through defective coordination on Zr_6 cluster. **b,** 3D representation of TTA-UC MOF structure with tunable Pd-TCPP to DCDPA ratio and schematic of TTA-UC process in the system. Defective sites (orange spheres) created by missing linkers, allowing the incorporation of Pd-TCPP. **c,** TEM image of TTA-UC MOF **5**. Scale bar = 100 nm. **d,** Comparison between simulated and experimental PXRD patterns of TTA-UC MOF **5**. **e,** Colloidal and photochemical stability of TTA-UC MOF **5** in water over one week. The UCL intensities at 440 nm were measured (λ_{ex} = 532 nm).

Synthesis and characterizations of TTA-UC MOFs. By varying the feed ratio of Pd-TCPP in the solvothermal synthesis of the MOF, DCDPA-based TTA-UC MOF nanoparticles with different Pd-TCPP concentrations were synthesized (namely, TTA-UC MOFs **1** – **9**). The synthesized TTA-UC MOFs show good dispersibility and colloidal stability in water for long-term storage (Figure 3a inset). Absorption spectra of TTA-UC MOFs dispersed in DMSO clearly reveal that the presence of both Pd-TCPP (at 417 and 523 nm) and DCDPA (at 356, 375, and 396 nm) with their characteristic bands (Supporting Information Figures S3–S5). Moreover, UV-Vis spectra, normalized to a constant concentration of DCDPA, confirmed that molar ratio of Pd-TCPP in DCDPA-based MOF nanoparticles is indeed tunable upon varying the feed ratio of Pd-TCPP (Figure 3a). In parallel, energy dispersive X-ray spectroscopy (EDS) and inductively coupled plasma atomic emission spectroscopy (ICP-AES) were carried out to confirm a quantitative trend of the varied Pd-TCPP contents in the TTA-UC MOFs. Due to the highly ordered and crystalline structure of TTA-UC MOF nanoparticles, the inserted Pd-TCPP contents can be calculated by comparing the elemental counts of Zr(IV) and Pd(II) of the MOF samples. Because the framework consists of DCDPA as the strut, each DCDPA linker corresponds to one Zr atom in an ideal **fcu** net. Although the insertion of Pd-TCPP on the Zr-cluster would slightly reduce the DCDPA to Zr ratio, the results were sufficient to see the trend due to the low content of Pd-TCPP compared to DCDPA.[24,29] According to the EDS and ICP-AES results, the ratio of Pd-TCPP to DCDPA in TTA-UC MOFs (samples **1** – **9**) decreases upon decreasing the dosing amount of Pd-TCPP in the synthesis (Supporting Information Tables S1 and S3), which shows an agreement with the trend in UV-Vis results. Therefore, the collective results confirm the controlled ratios of the annihilator and sensitizer in our TTA-UC MOF system.

TTA-UC luminescence (UCL) spectra of TTA-UC MOFs **1** – **9** were then obtained in water (Figure 3b) to screen the best performing TTA-UC. UCL intensity of the samples with the extremely low contents of Pd-TCPP (samples **7** – **9**) is attenuated presumably due to the insufficient TTET contribution. While increasing Pd-TCPP in the MOFs, it led to a much improved UCL intensity as shown in **5**. However, further increase of Pd-TCPP rather resulted in a decreasing trend in UCL intensity (samples **1** – **4**). Such decrement can be attributed to the inner-filter effect (re-absorption), caused by partial spectral overlap between strong absorption from Soret band of Pd-TCPP (λ_{abs} = 417 nm) and the UCL emission of DCDPA, resulting in a decreased UCL intensity as well as an apparent red-shift of UCL peaks in these samples (Figure 3b).[30] These results indeed show the advantage of our TTA-UC platform that allows the fine-tuning of the annihilator/sensitizer ratio for screening the best TTA-UC performer.

Subsequently, TTA-UC MOF **5**, optimized for the best TTA-UC performance, was further characterized. Transmission electron microscopy (TEM) confirmed that the size of the TTA-UC MOF **5** is ~55 nm with octahedral morphology (Figure 2c). Powder X-ray diffraction showed the experimental diffractions match well with that of calculated UiO-68 (Figure 2d). Interestingly, although the anthracene core is known to be highly hydrophobic, dynamic light scattering (DLS) confirmed that **5** can be well dispersed and stabilized in water in the absence of additional surfactant (Supporting Information Figure S7). These results show a good agreement with our previous observations where the 3D porous structure of the MOF could lead to a much decreased surface contact between particles thus stabilizing the MOF nanoparticles.[31] In addition, PXRD shows the robust Zr(IV)-carboxylate bonds can support intactness of the framework in aqueous media over a week (Supporting Information Figure S9). Aside from the chemical stability of our Zr-based MOF, the aqueous suspension of **5** was also tested for the colloidal stability and luminescence properties. It was confirmed that no obvious changes were found in hydrodynamic size as indicated from the DLS measurements, while only a negligible decrease in the UCL intensity was observed perhaps due to the photo-oxidation common in these systems (Figure 2e). These results clearly support the unique nature of our MOF nanoplatform indeed enables a long-term stability of TTA-UC MOF in water.

Next, incident laser power dependence on UCL was studied in an aqueous suspension of sample **5** (Supporting Information Figure S10). Figure 3c shows a quadratic-to-linear dependence of TTA-UC MOF **5** (slopes = 1.90 and 0.91, respectively) between the UCL intensity and the excitation power density, which is an indicative feature of the typical TTA-UC system. The threshold of excitation power density (I_{th}, revealed as an intersection of these two slopes in Figure 3c) was determined to be as low as 2.5 mW cm^{-2} that is close to the level of solar irradiance at 532 ± 10 nm, suggesting a saturation of TTA-UC quantum yield at low-power excitation.[11,32] Then, UCL quantum efficiency (Φ_{UCL}) of TTA-UC MOF **5** was measured in aerated water referenced to $Ru(bpy)_3Cl_2$ (Supporting Information Figure S11).[33] To the best of our knowledge, TTA-UC MOF **5** shows the highest UCL quantum efficiency (Φ_{UCL} = 1.28±0.07%) under excitation at 2.5 mW cm^{-2}, among that of the reported TTA-UC systems measured in aqueous media.[14,34-39] Such high efficiency can also be attributed to efficient TTA process arising from the intimate distance between adjacent anthracene cores (about 5.6 Å based on C–C) (Supporting Information Scheme S2b) aside from the structural design in our TTA-UC MOF that has been previously mentioned. Meanwhile, the highly ordered alignment of the immobilized annihilators in the TTA-UC MOF offers the efficient exciton diffusion with less rotational freedom within the framework, significantly reducing the non-radiative decay pathways.[40-41] Therefore, a long UCL lifetime (τ_{UCL}) of 1.6 ms was observed in TTA-UC MOF **5**, which is even much longer than that of the reported TTA-UC systems in organic solvents (~100 μs) (Figure 3d).[42-43] In particular, τ_{UCL} measured in aerated water did not show a noticeable difference compared with that in nitrogen atmosphere. This indicates that our system is not much sensitive to oxygen, which is desirable for

our application. The insensitivity to oxygen was probably due to hydrophobic environment, generated from the dense anthracene-based molecular alignment in the TTA-UC MOF.[36]

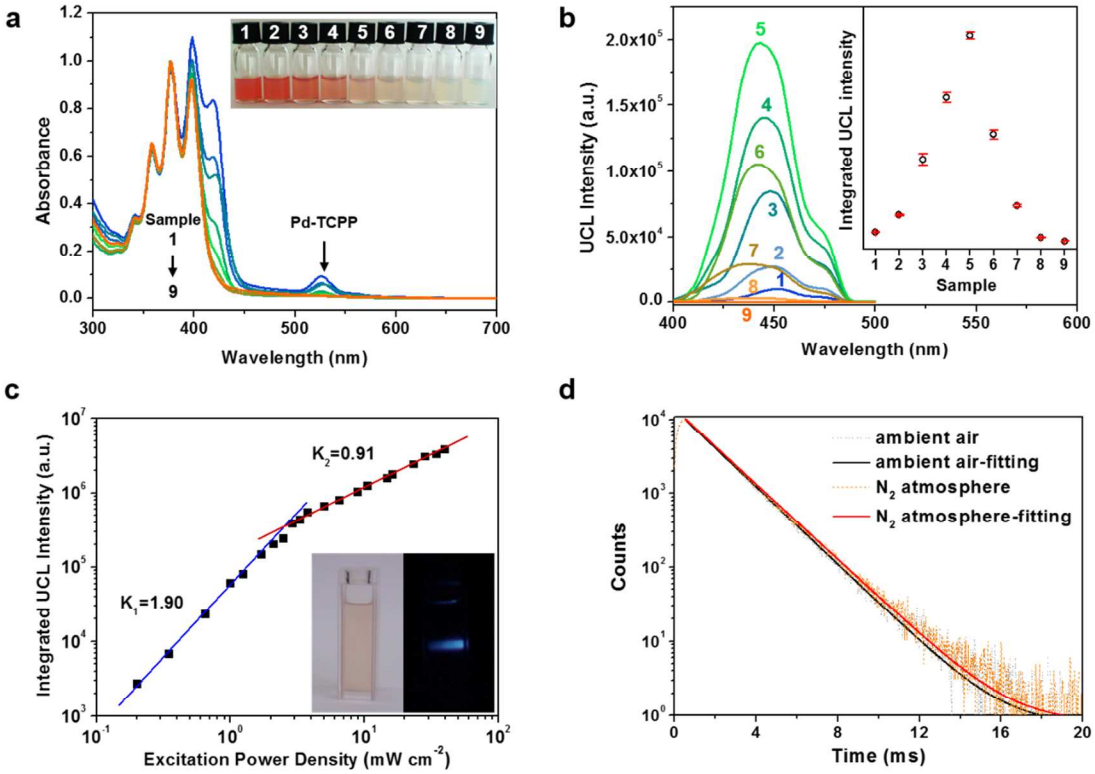

Figure 3 | Photophysical characterizations of TTA-UC MOFs. a, UV-Vis spectra of TTA-UC MOFs **1** – **9** in water. The spectra were normalized at 375 nm and the decreasing trend of Pd-TCPP concentration was highlighted with an arrow around 532 nm. Inset: Photographs of the MOF samples in water. The picture was taken 15 months after the samples were synthesized and stored in a dark container, showing good water dispersibility. **b,** UCL spectra of TTA-UC MOFs **1** – **9** in water (λ_{ex} = 532 nm at 20 mW cm^{-2}). A 530 nm short-pass filter was used to cut off the excitation laser. Inset: Integrated UCL intensity of the MOFs samples. **c,** Integrated UCL intensity of the optimized TTA-UC MOF **5** as a function of 532 nm excitation power density in water. Inset: bright field (left) and UCL images under 532 nm laser excitation (2.5 mW cm^{-2}, right) of TTA-UC MOF **5**. A 530 nm short-pass filter was used to cut off the excitation laser. **d,** TTA-UC lifetime measurement of TTA-UC MOF **5** in water. The samples were measured in the ambient air (black) and in N_2 atmosphere (red), respectively.

To further explore the mechanism, the process of energy migration was subsequently investigated. The triplet diffusion related parameters of TTA-UC MOF **5** in water were theoretically determined according to the following equations, where α is the absorption coefficient at 532 nm excitation in wavenumber, τ_T is the lifetime of the acceptor triplet, γ_{TT} is the second-order annihilation constant for the TTA, a_o is the annihilation distance of the triplets.

$$I_{th} = \frac{1}{\alpha \emptyset_{TTET} \gamma_{TT} \sqrt{\tau_T}} \quad \text{(Eq. 1)}$$

$$\tau_T = 2\tau_{UCL} \quad \text{(Eq. 2)}$$

$$D_T = \frac{\gamma_{TT}}{8\pi a_0} \quad \text{(Eq. 3)}$$

$$L_T = \sqrt{D_T \tau_T} \quad \text{(Eq. 4)}$$

Consequently, TTA-UC MOF **5** shows a calculated triplet exciton diffusion constant (D_T) of 7.7 × 10^{-6} cm^2 s^{-1} and diffusion length (L_T) of 1.6 μm (Supporting Information Section 9).[44-45] Markedly, the triplet diffusion in water is as fast as that in low-viscous organic solvents.[10] Moreover, the average nearest-neighboring distance between two sensitizers was calculated to be 26.5 nm by using the stochastic algorithm from the concentration of the sensitizer.[46] This value indicates that the long-range triplet diffusion of 1.6 μm in water is far enough to cover the average distance between two sensitizers (26.5 nm) and the size of the TTA-UC MOF **5** nanoparticle (~55 nm), which enables the efficient triplet energy migration in sample **5**. There-

fore, the fast and long-range triplet energy migration in TTA-UC MOF greatly promotes the TTA-UC performance in water. Such remarkable results achieved by our MOF formulation indeed suggest that our system is beneficial for TTA-UC based biomedical applications in aqueous environments.

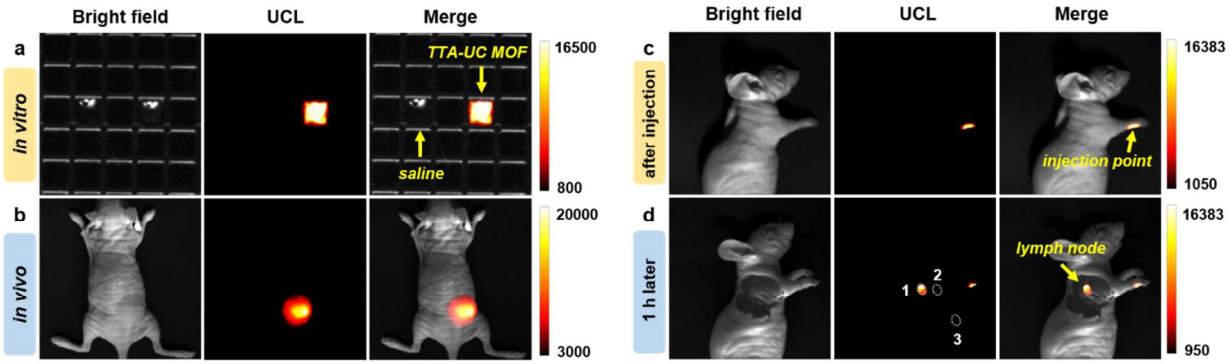

Figure 4 | *In vitro* and *in vivo* imaging of TTA-UC MOF 5. a, *in vitro* and **b,** *in vivo* imaging with TTA-UC MOF **5** (λ_{ex} = 532 nm at 20 mW cm^{-2}). *In vitro* imaging was carried out by filling TTA-UC MOF **5** in the 384-well plates. 200 μL of TTA-UC MOF **5** (2 mg mL^{-1}) was subcutaneously injected to a nude mouse. The images were taken 10 min after the injection. **c-d,** *in vivo* lymph node imaging with TTA-UC MOF **5** (λ_{ex} = 532 nm at 5 mW cm^{-2}). 100 μL of TTA-UC MOF **5** (2 mg mL^{-1}) was injected in footpad of forepaw. The images were taken at 5 min and 1 h after the injection, respectively. SNR = $(I_1-I_2)/(I_2-I_3)$ = 31, where I_1, I_2 and I_3 refer to the mean UCL intensity of regions 1, 2, and 3, respectively.

Low-power bioimaging *in vivo* based on TTA-UC MOF nanoparticles. To employ our concept to biological imaging studies, we first investigated the photostability of sample **5** using kinetic scan assay under continuous laser excitation (λ_{ex} = 532 nm). Notably, TTA-UC MOF **5** showed no significant photo-degradation even under intense laser irradiation (100 mW cm^{-2}) during the measurement, implying its applicability for real-time imaging application (Supporting Information Figure S13). Prior to *in vivo* imaging, cytotoxicity of **5** was also tested with HeLa cells, which showed no significant cytotoxicity (Supporting Information Figure S14).[15,47] Then the upconversion performance of TTA-UC MOF **5** was tested with our homebuilt bioimaging instrument.[48] As shown in *in vitro* imaging, an intense upconverted luminescence of TTA-UC MOF **5** collected at 450 ± 25 nm (blue emission channel) was observed upon excitation at 532 nm while no signal was detected from the blank sample of saline (Figure 4a). Next, the sample **5** was subcutaneously injected into a nude mouse while the saline was subcutaneously injected to another mouse as a control (Supporting Information Figure S15). Ten minutes after the injection, the imaging was conducted under identical conditions. While the control mouse showed no noticeable TTA-UC response *in vivo* in the blue emission channel, the mouse with TTA-UC MOF **5** injected exhibited strong upconversion fluorescence with high imaging contrast (SNR of ~45 at 20 mW cm^{-2}) despite the nature of moderate penetration from visible light excitation (Figure 4b). Both *in vitro* and *in vivo* results indicate that the Zr-MOF nanoplatform was successfully employed to demonstrate TTA-UC for bioimaging.

We then further pursued an imaging of lymph node because the sentinel node of lymphatic system is known to be correlated with tumor metastasis.[49] Thus, the lymph node imaging is important to the pathologic staging and lymphadenectomy. Real-time imaging of the lymph node was performed with the injection of TTA-UC MOF **5** into forepaw footpad of a nude mouse. In Figure 4c, the upconversion response distributed around the injection point was clearly observed right after the injection upon irradiation at 532 nm laser (5 mW cm^{-2}). Along with the transfer of TTA-UC MOF **5**, the sentinel node was lit up by upconversion fluorescence in 1 h (Figure 4d). It is worth noting that SNR of ~31 was achieved *in vivo* at very low excitation power density of 5 mW cm^{-2}. We also confirmed that after the imaging with **5**, no histologic abnormality of the lymph node was observed from the hematoxylin and eosin (H&E) stain result (Supporting Information Figure S16). Therefore, the TTA-UC MOF indeed demonstrates as a promising nanoplatform to enable the feasibility of upconversion technique in practical imaging applications.

CONCLUSION

In summary, through the *in situ* incorporation strategy of multiple functionalities into the Zr-MOF, a MOF-based tunable TTA-UC system was achieved for low-power *in vivo* imaging. The TTA dyad loaded water-stable/dispersible TTA-UC MOF nanoparticles show remarkable TTA-UC luminescence quantum efficiency as high as 1.28% in water. In particular, a long-range triplet diffusion of 1.6 μm in water was also achieved by the well-aligned annihilators in the MOF platform. The TTA-UC MOF with the optimized ratio of sensitizer to annihilator

was employed for *in vivo* imaging of a live mouse exhibiting an excellent SNR of ~45. Furthermore, the TTA-UC MOF successfully demonstrated the lymph node imaging of a live mouse *in vivo* with excellent SNR (> 30) at very low power density (5 mW cm^{-2}). Our findings show a great promise that our TTA-UC MOF combined with the fine-tuning ability can serve as an ideal host system for TTA-UC dyad for *in vivo* bioimaging. We also envision that surface modification of these MOF nanoparticles can further improve the system enabling targeting and theranostic functions.

EXPERIMANTAL SECTION

TTA-UC MOF synthesis. In a 20 mL Pyrex vial, DCDPA (30 mg, 0.072 mmol), zirconyl chloride octahydrate ($ZrOCl_2 \cdot 8H_2O$) (30 mg, 0.093 mmol), Pd-TCPP (see Table S1 for varied amounts), and acetic acid (120 μL) were ultrasonically dissolved in 6 mL of *N,N*-dimethylformamide (DMF). The reaction mixture was stirred (300 rpm) for 3 h at 90 °C. The resulting nanoparticles were collected by centrifugation (17000 rpm, 30 min) followed by sequential washing with fresh DMF and dimethyl sulfoxide (DMSO) for three times, respectively. The resulting nanoparticles were suspended in DMSO for further characterization and analysis unless otherwise noted where relevant.

Upconversion quantum efficiency measurement. TTA-upconversion quantum efficiency (Φ_{UCL}) of TTA-UC MOF samples in water was determined by relative quantum yield measurement. $Ru(bpy)_3Cl_2$ in water was used as the standard reference (absolute quantum efficiency Φ_{Ref} = 0.040 in aerated H_2O).[32] A 532 nm laser was used as excitation source for both of TTA-UC MOF and $Ru(bpy)_3Cl_2$. The TTA-upconversion quantum efficiency was calculated with the equation below.[5-6] $\Phi_{UCL} = 2\Phi_{Ref}(A_{Ref}/A)(I/I_{Ref})(\eta/\eta_{Ref})$ where A is the absorption at 532 nm, I is the emission intensity, η is the refraction of water. The multiplicative factor of 2 was reflected to represent the TTA mechanism (bimolecular process).

***In vivo* imaging.** The animal procedures were in accordance with the guidelines of the Institutional Animal Care and Use Committee, School of Pharmacy, Fudan University. TTA-upconversion luminescence imaging *in vivo* was performed with an imaging system designed by the Li group at Fudan University. An EMCCD (Andor, DU897) was used as the signal detector and a 530 nm short pass filter was additionally used to cut off the 532 nm excitation laser light. Nude mice were used for the *in vivo* experiments, and TTA-UC MOF samples were dispersed in PBS. For the subcutaneous model, the imaging was performed at 10 minutes post-injection of TTA-UC MOF under the excitation of 532 nm laser (20 mW cm^{-2}). While in the case of lymph node model, the TTA-UC MOF were injected in the footpad of forepaw 1 h before the imaging under the excitation of 532 nm (5 mW cm^{-2}). Upconversion emission at the blue emission channel (450 ± 25 nm) was collected for all the imaging applications.

ASSOCIATED CONTENT

Supporting Information

Synthesis and characterization of TTA-UC MOFs are shown in the supporting information. The theoretical calculations are also included. This material is available free of charge *via* the Internet at http: //pubs.acs.org.

AUTHOR INFORMATION

Corresponding Authors

zhou@chem.tamu.edu (H. C. Zhou)

fyli@fudan.edu.cn (F. Y. Li)

Author Contributions

†These authors contributed equally to this work.

Jihye Park & Ming Xu

§ Present address: Department of Chemical Engineering, Stanford University, Stanford, CA 94305, USA

Notes

The authors declare no competing financial interest.

Acknowledgment

H.-C.Z. acknowledges the support from the Welch Foundation (A-0030). MOST of China (2015CB931801) and National Natural Science Foundation of China (201375024 and 201375024) are acknowledged. The authors gratefully acknowledge Dr. Dawei Feng for fruitful discussion, Dr. Zhangwen Wei for graphics, and Mrs. Wei Yuan for assistance in bioimaging.

REFERENCES

(1) Auzel, F. *Chem. Rev.* **2004,** *104*, 139-173.
(2) Zhou, J.; Liu, Z.; Li, F. *Chem. Soc. Rev.* **2012,** *41*, 1323-1349.
(3) Wang, F.; Liu, X. *Chem. Soc. Rev.* **2009,** *38*, 976-989.
(4) Chen, G.; Qiu, H.; Prasad, P. N.; Chen, X. *Chem. Rev.* **2014,** *114*, 5161-5214.
(5) Zhou, J.; Liu, Q.; Feng, W.; Sun, Y.; Li, F. *Chem. Rev.* **2015,** *115*, 395-465.
(6) Singh-Rachford, T. N.; Castellano, F. N. *Coord. Chem. Rev.* **2010,** *254*, 2560-2573.
(7) Oldenburg, M.; Turshatov, A.; Busko, D.; Wollgarten, S.; Adams, M.; Baroni, N.; Welle, A.; Redel, E.; Woll, C.; Richards, B. S.; Howard, I. A. *Adv. Mater.* **2016,** *28*, 8477-8482.
(8) Yanai, N.; Kimizuka, N. *Chem. Comm.* **2016,** *52*, 5354-5370.
(9) Wang, F.; Deng, R.; Wang, J.; Wang, Q.; Han, Y.; Zhu, H.; Chen, X.; Liu, X. *Nat. Mater.* **2011,** *10*, 968-973.
(10) Monguzzi, A.; Tubino, R.; Meinardi, F. *Phys. Rev. B* **2008,** *77*, 155122.
(11) Monguzzi, A.; Mezyk, J.; Scotognella, F.; Tubino, R.; Meinardi, F. *Phys. Rev. B* **2008,** *78, 195112*.
(12) Wohnhaas, C.; Turshatov, A.; Mailaender, V.; Lorenz, S.; Baluschev, S.; Miteva, T.; Landfester, K. *Macromol. Biosci.* **2011,** *11*, 772-778.
(13) Kwon, O. S.; Song, H. S.; Conde, J.; Kim, H. I.; Artzi, N.; Kim, J. H. *ACS Nano* **2016,** *10*, 1512-1521.
(14) Liu, Q.; Yin, B.; Yang, T.; Yang, Y.; Shen, Z.; Yao, P.; Li, F. *J. Am. Chem. Soc.* **2013,** *135*, 5029-5037.
(15) He, C.; Liu, D.; Lin, W. *Chem. Rev.* **2015,** *115*, 11079-11108.

(16) Williams, D. E.; Rietman, J. A.; Maier, J. M.; Tan, R.; Greytak, A. B.; Smith, M. D.; Krause, J. A.; Shustova, N. B. *J. Am. Chem. Soc.* **2014,** *136*, 11886-11889.
(17) Lee, C. Y.; Farha, O. K.; Hong, B. J.; Sarjeant, A. A.; Nguyen, S. T.; Hupp, J. T. *J. Am. Chem. Soc.* **2011,** *133*, 15858-15861.
(18) Kent, C. A.; Liu, D.; Ma, L.; Papanikolas, J. M.; Meyer, T. J.; Lin, W. *J. Am. Chem. Soc.* **2011,** *133*, 12940-12943.
(19) Fateeva, A.; Chater, P. A.; Ireland, C. P.; Tahir, A. A.; Khimyak, Y. Z.; Wiper, P. V.; Darwent, J. R.; Rosseinsky, M. J. *Angew. Chem. Int. Ed.* **2012,** *51*, 7440-7444.
(20) Park, J.; Jiang, Q.; Feng, D.; Zhou, H. C. *Angew. Chem. Int. Ed.* **2016,** 55, 7188-7193.
(21) Furukawa, H.; Ko, N.; Go, Y. B.; Aratani, N.; Choi, S. B.; Choi, E.; Yazaydin, A. Ö.; Snurr, R. Q.; O'Keeffe, M.; Kim, J.; Yaghi, O. M. *Science* **2010,** *329*, 424.
(22) Haefele, A.; Blumhoff, J.; Khnayzer, R. S.; Castellano, F. N. *J. Phys. Chem. Lett.* **2012,** *3*, 299-303.
(23) Ma, B. Q.; Mulfort, K. L.; Hupp, J. T. *Inorg. Chem.* **2005,** *44*, 4912-4914.
(24) Wu, H.; Chua, Y. S.; Krungleviciute, V.; Tyagi, M.; Chen, P.; Yildirim, T.; Zhou, W. *J. Am. Chem. Soc.* **2013,** *135*, 10525-10532.
(25) Trickett, C. A.; Gagnon, K. J.; Lee, S.; Gandara, F.; Burgi, H. B.; Yaghi, O. M. *Angew. Chem. Int. Ed.* **2015,** *54*, 11162-11167.
(26) Taylor, J. M.; Komatsu, T.; Dekura, S.; Otsubo, K.; Takata, M.; Kitagawa, H. *J. Am. Chem. Soc.* **2015,** *137*, 11498-11506.
(27) Cliffe, M. J.; Wan, W.; Zou, X.; Chater, P. A.; Kleppe, A. K.; Tucker, M. G.; Wilhelm, H.; Funnell, N. P.; Coudert, F.-X.; Goodwin, A. L. *Nat. Commun.* **2014,** *5*, 4176.
(28) Börjesson, K.; Rudquist, P.; Gray, V.; Moth-Poulsen, K. *Nat. Commun.* **2016,** *7*, 12689.
(29) Sun, Y.; Sun, L.; Feng, D.; Zhou, H. C. *Angew. Chem. Int. Ed.* **2016,** 55, 6471-6475.
(30) Deng, F.; Blumhoff, J.; Castellano, F. N. *J. Phys. Chem. A* **2013,** *117*, 4412-4419.
(31) Park, J.; Jiang, Q.; Feng, D.; Mao, L.; Zhou, H.-C. *J. Am. Chem. Soc.* **2016,** *138*, 3518-3525.
(32) Cheng, Y. Y.; Fuckel, B.; Khoury, T.; Clady, R. G. C. R.; Tayebjee, M. J. Y.; Ekins-Daukes, N. J.; Crossley, M. J.; Schmidt, T. W. *J. Phys. Chem. Lett.* **2010,** *1*, 1795-1799.
(33) Suzuki, K.; Kobayashi, A.; Kaneko, S.; Takehira, K.; Yoshihara, T.; Ishida, H.; Shiina, Y.; Oishic, S.; Tobita, S. *Phys. Chem. Chem. Phys.* **2009,** *11*, 9850-9860.
(34) Monguzzi, A.; Frigoli, M.; Larpent, C.; Tubino, R.; Meinardi, F. *Adv. Funct. Mater.* **2012,** *22*, 139-143.
(35) Mattiello, S.; Monguzzi, A.; Pedrini, J.; Sassi, M.; Villa, C.; Torrente, Y.; Marotta, R.; Meinardi, F.; Beverina, L. *Adv. Funct. Mater.* **2016,** *26*, 8447-8454.
(36) Kouno, H.; Ogawa, T.; Amemori, S.; Mahato, P.; Yanai, N.; Kimizuka, N. *Chem. Sci.* **2016,** *7*, 5224-5229.
(37) Kim, J. H.; Kim, J. H. *ACS Photonics* **2015,** *2*, 633-638.
(38) Kim, J. H.; Kim, J. H. *J. Am. Chem. Soc.* **2012,** *134*, 17478-17481.
(39) Askes, S. H. C.; Pomp, W.; Hopkins, S. L.; Kros, A.; Wu, S.; Schmidt, T.; Bonnet, S. *Small* **2016,** *12*, 5579-5590.
(40) Wei, Z.; Gu, Z.-Y.; Arvapally, R. K.; Chen, Y.-P.; McDougald, R. N.; Ivy, J. F.; Yakovenko, A. A.; Feng, D.; Omary, M. A.; Zhou, H.-C. *J. Am. Chem. Soc.* **2014,** *136*, 8269-8276.
(41) Shustova, N. B.; Ong, T.-C.; Cozzolino, A. F.; Michaelis, V. K.; Griffin, R. G.; Dincă, M. *J. Am. Chem. Soc.* **2012,** *134*, 15061-15070.
(42) Zhao, J.; Wu, W.; Sun, J.; Guo, S. *Chem. Soc. Rev.* **2013,** *42*, 5323-5351.
(43) Zhao, J. Z.; Ji, S. M.; Guo, H. M. *RSC Adv.* **2011,** *1*, 937-950.
(44) Monguzzi, A.; Tubino, R.; Hoseinkhani, S.; Campione, M.; Meinardi, F. *Phys. Chem. Chem. Phys.* **2012,** *14*, 4322-4332.
(45) Thevenaz, D. C.; Monguzzi, A.; Vanhecke, D.; Vadrucci, R.; Meinardi, F.; Simon, Y. C.; Weder, C. *Mater. Horiz.* **2016,** *3*, 602-607.
(46) Ito, A.; Stewart, D. J.; Knight, T. E.; Fang, Z.; Brennaman, M. K.; Meyer, T. J. *J. Phys. Chem. B* **2013,** *117*, 3428-3438.
(47) Li, Y.; Tang, J.; He, L.; Liu, Y.; Liu, Y.; Chen, C.; Tang, Z. *Adv. Mater.* **2015,** *27*, 4075-4080.
(48) Xiong, L.; Chen, Z.; Tian, Q.; Cao, T.; Xu, C.; Li, F. *Anal. Chem.* **2009,** *81*, 8687-8694.
(49) Krag, D.; Weaver, D.; Ashikaga, T.; Moffat, F.; Klimberg, V. S.; Shriver, C.; Feldman, S.; Kusminsky, R.; Gadd, M.; Kuhn, J.; Harlow, S.; Beitsch, P. *New Engl. J. Med.* **1998,** *339*, 941-946.

Table of Contents Graphic